Hyperbolic Dispersion Arising from Anisotropic Excitons in Two-Dimensional Perovskites

Peijun Guo,[1] Wei Huang,[2,3] Constantinos C. Stoumpos,[2] Lingling Mao,[2] Jue Gong,[4] Li Zeng,[5] Benjamin T. Diroll,[1] Yi Xia,[1] Xuedan Ma,[1] David J. Gosztola,[1] Tao Xu,[4] John B. Ketterson,[6] Michael J. Bedzyk,[5,6,7] Antonio Facchetti,[2,8] Tobin J. Marks,[2,3] Mercouri G. Kanatzidis,[2] and Richard D. Schaller[1,2,*]

[1]*Center for Nanoscale Materials, Argonne National Laboratory, 9700 South Cass Avenue, Lemont, Illinois 60439, USA*
[2]*Department of Chemistry, Northwestern University, 2145 Sheridan Road, Evanston, Illinois 60208, USA*
[3]*Materials Research Center, Northwestern University, 2145 Sheridan Road, Evanston, Illinois 60208, USA*
[4]*Department of Chemistry & Biochemistry, Northern Illinois University, DeKalb, Illinois 60115, USA*
[5]*Applied Physics Program, Northwestern University, 2145 Sheridan Road, Evanston, Illinois 60208, USA*
[6]*Department of Physics and Astronomy, Northwestern University, 2145 Sheridan Road, Evanston, Illinois 60208, USA*
[7]*Department of Materials Science and Engineering, Northwestern University, 2145 Sheridan Road, Evanston, Illinois 60208, USA*
[8]*Flexterra Corporation, 8025 Lamon Avenue, Skokie, Illinois 60077, USA*

(Received 13 March 2018; published 19 September 2018)

Excitations of free electrons and optical phonons are known to permit access to the negative real part of relative permittivities ($\varepsilon' < 0$) that yield strong light-matter interactions. However, negative ε' arising from excitons has been much less explored. Via development of a dielectric-coating based technique described herein, we report fundamental optical properties of two-dimensional hybrid perovskites (2DHPs), composed of alternating layers of inorganic and organic sublattices. Low members of 2DHPs ($N = 1$ and $N = 2$) exhibit negative ε' stemming from the large exciton binding energy and sizable oscillator strength. Furthermore, hyperbolic dispersion (i.e., ε' changes sign with directions) occurs in the visible range, which has been previously achieved only with artificial metamaterials. Such naturally occurring, exotic dispersion stems from the extremely anisotropic excitonic behaviors of 2DHPs, and can intrinsically support a large photonic density of states. We suggest that several other van der Waals solids may exhibit similar behaviors arising from excitonic response.

DOI: 10.1103/PhysRevLett.121.127401

Excitons are bound electron-hole pairs that represent one kind of elementary electronic excitation in materials with screened Coulomb interactions [1]. Excitons, similar to plasmons (collective oscillations of free electrons) and optical phonons (collective lattice vibrations), can strongly couple with electromagnetic waves in the form of polaritons [2–5]. At optical frequencies, the interaction between matter and electromagnetic waves is encoded into the relative permittivity ($\varepsilon = \varepsilon' + i\varepsilon''$). Extensive studies on surface plasmon polaritons and surface phonon polaritons [6,7] rely on ε' values that are below zero, which is essential for the confinement of light at subwavelength scales, and enables numerous applications ranging from solar energy harvesting to ultrasensitive biosensing [8,9]. Furthermore, hyperbolic dispersion, that is, ε' exhibiting different signs along different directions, which manifests extreme optical anisotropy, has been achieved with both plasmonic and phononic responses [4,10]. Obtaining such a regime of ε' with excitons, however, is much more challenging, due to a very limited number of bulk materials exhibiting strong excitonic effects and large optical anisotropy simultaneously. The recently reemerged 2DHPs show extreme and tunable quantum-confinement effects [11–16], and share the same layered structure as both artificially grown metal-dielectric superlattices [17] and van der Waals materials such as *h*-BN [4]. Here, we show that exciton-induced negative ε' and hyperbolic dispersion ($\varepsilon' < 0$ in the in-plane direction, and $\varepsilon' > 0$ in the out-of-plane direction) can be realized in 2DHPs. The similarity between excitons and other fundamental excitations, and their effect on anisotropic ε demonstrated in this work is crucial for novel optoelectronic and nanophotonic applications utilizing 2DHPs and other quantum-well-like materials.

The macroscopic, single crystals of 2DHPs examined here comprise chemical compositions of $(BA)_2(MA)_{N-1}Pb_NI_{3N+1}$, where $N = 1$ to 4, $BA = CH_3(CH_2)_3NH_3^+$, and $MA = CH_3NH_3^+$ [Fig. 1(a)]. The interdigitating $(BA)_2^{2+}$ organic cations, which separate the Pb-I octahedral sheets that expand in two dimensions, give rise to strong quantum and dielectric confinement effects. Although orthorhombic [18], these materials can be well approximated as uniaxial crystals [14] with the optic axis pointing along $\vec{c}$, due to the negligibly different (<1%) lattice constants along $\vec{a}$ and $\vec{b}$. The ε tensor is written as

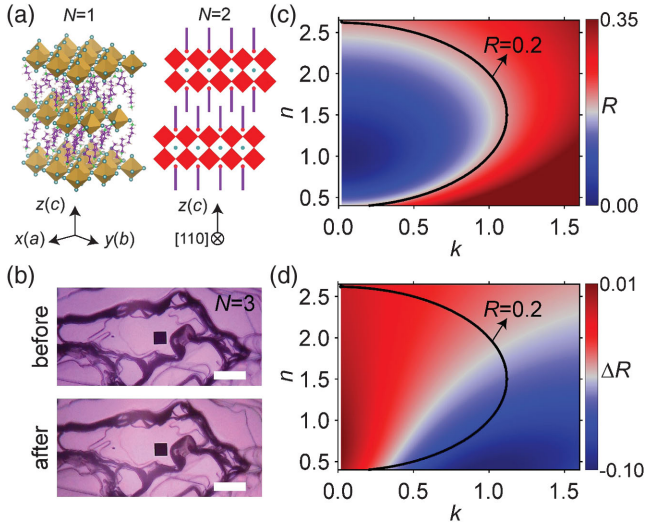

FIG. 1. (a) Schematic of the crystal structures of $N = 1$ (left, 3D view) and $N = 2$ (right, 2D view). (b) Optical micrographs of an $N = 3$ single crystal flake before and after coating with MoO_x, viewed along $\vec{c}$. The reflectivity spectrum was acquired from the region indicated by the black square. The white scale bar is 40 μm. (c) Calculated dependence of reflectivity (R; color-coded) on the values of n and k of an infinitely-thick, optically absorbing medium. (d) Calculated change of reflectivity (ΔR; color-coded) as a function of n and k of an optically absorbing medium, due to an 11-nm thick coating of MoO_x. Both (c) and (d) are calculated for normal incidence, with a representative contour of $R = 0.2$ plotted.

$$\begin{pmatrix} \varepsilon_{xx} & 0 & 0 \\ 0 & \varepsilon_{yy} & 0 \\ 0 & 0 & \varepsilon_{zz} \end{pmatrix},$$

where $\varepsilon_{xx} = \varepsilon_{yy} \neq \varepsilon_{zz}$, and x, y, and z are defined to be parallel to the $\vec{a}$, $\vec{b}$, and $\vec{c}$ axes, respectively [Fig. 1(a)]. Previous studies on the refractive index (RI) of 2DHPs were limited to polycrystalline thin films [19]. Because the surfaces of 2DHP single crystal flakes are only microscopically smooth [Fig. 1(b)], techniques such as spectroscopic ellipsometry are problematic. Although microscopic reflection measurements at normal incidence can be performed on locally smooth, single-crystal-quality surfaces [20], the reflectivity (R) of an absorbing medium, with a thickness that significantly exceeds the optical penetration depth (so that light is completely attenuated, and no reflection from the bottom surface of the crystal takes place), depends (only) on both real (n) and imaginary part (k) of the RI. Figure 1(c) presents the calculated R as a function of n and k for an infinitely thick, optically absorbing medium. Evidently, a single reflection measurement is insufficient to constrain both n and k. A Kramers-Kronig analysis to infer both n and k from a single reflection measurement is challenging because spectral weights of the inorganic and organic sublattices cover a wide range from the ultraviolet to the near- and midinfrared.

To solve this problem, we use the fact that an ultrathin ($\ll\lambda/4$ where λ is the wavelength) dielectric coating on an absorbing medium (here being the 2DHP single crystals) produces nontrivial phase shift at the interface [21], and with it a sizable ΔR, where ΔR is the change of reflection due to the coating. Note that the examined 2DHP single crystals here are tens to hundreds of micrometers thick, and so are orders-of-magnitude thicker than the above-band-gap optical penetration depth, which is on the order of tens to hundreds of nanometers, such that the 2DHP crystals can be considered "infinitely" thick. Figure 1(d) illustrates the calculated dependence of ΔR on the n and k values of the infinitely thick medium due to the coating of an ultrathin dielectric layer with known RI (plotted in the Supplemental Material, Fig. S1 [22]) and thickness (11 nm), using a transfer-matrix approach. Because points on the contour in Fig. 1(c) (with constant R) are associated with different values of ΔR in Fig. 1(d), we can unambiguously determine n and k at each wavelength by solving an inverse problem using R and ΔR as input parameters, without invoking any phenomenological models or the associated fitting parameters. Although combining microscopic transmission and reflection measurements at normal incidence of an optically thin 2DHP crystal, with known thickness, can in principle permit the determination of RI, such an approach may only yield RI along the in-plane direction. This arises because 2DHPs can only be exfoliated by breaking the van der Waals bonds between the layers, which results in a layer parallel to the perovskite sheets, and, as a result, ε along the cross-plane direction cannot be readily accessed. Our proposed technique is suitable for any optically absorbing media (e.g., in the above band-gap region of a semiconductor) that are spatially smooth over length scales on the order of several wavelengths (i.e., ultimately diffraction limited), and hence can be applied to the emerging supermolecular single crystals [34] and exfoliated 2D TMDs [35], with achievable sizes typically below tens of microns.

Thermal evaporation, as a nonenergetic process (to minimize sample damage), was employed to coat thin layers of MoO_x, which has a low melting point. Thickness and RI of the evaporated MoO_x film, which showed negligible substrate dependence, were extracted from x-ray reflectivity and ellipsometric measurements (Supplemental Material, Figs. S1 and S2 [22]). Figure 2(a) presents the measured R for $N = 1$ to $N = 4$, and ΔR (see Supplemental Material, Fig. S3 [22] for reflection after the coating) following an 11-nm coating of MoO_x, measured with $\boldsymbol{k} \| \vec{c}$ where $\boldsymbol{k}$ is the wave vector of light. The determined n and k for $N = 1$ to $N = 4$ along the ab plane are plotted in Figs. 2(b) and 2(c), respectively. We also determined n and k for several three-dimensional (3D) perovskites, including $MAPbCl_3$, $MAPbBr_3$, and $CsPbBr_3$ (Supplemental Material, Figs. S4 to S6 [22]), using the same method, and the results agree well with an earlier report based on ellipsometric measurements [36]. Note that the more regular shape and larger

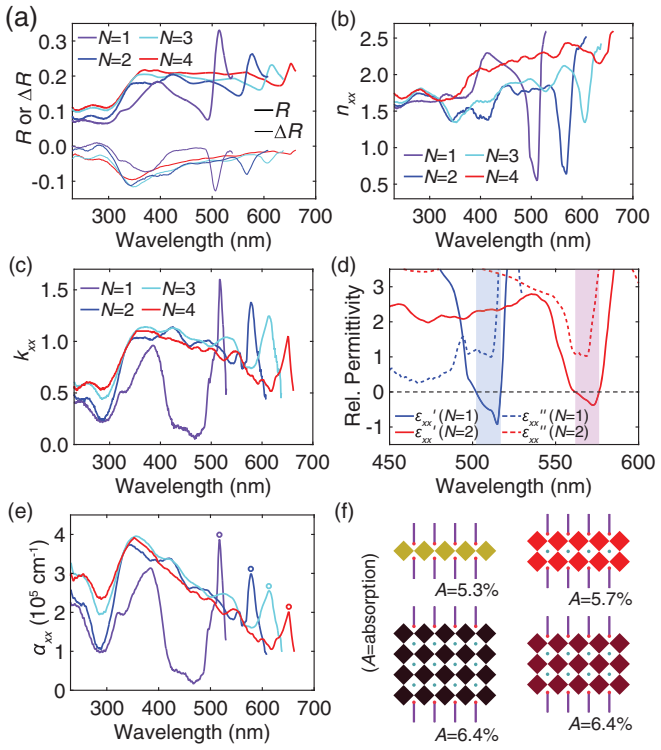

FIG. 2. (a) R and ΔR (after the coating with 11-nm thick MoO_x) measured with $\boldsymbol{k}\|\vec{c}$ for $N = 1$ to $N = 4$. (b) In-plane n and (c) k for $N = 1$ to $N = 4$. (d) In-plane ε' and ε'' for $N = 1$ and $N = 2$. The colored areas highlight the spectral regions of $\varepsilon' < 0$ (blue for $N = 1$ and red for $N = 2$). (e) In-plane α for $N = 1$ to $N = 4$. (f) Light absorption by $N = 1$ to $N = 4$ at the corresponding exciton resonant wavelengths indicated by the circles in (e).

available sizes of 3D perovskite single crystals are compatible with spectroscopic ellipsometry. For 2DHPs, the strength of the excitonic resonance, manifested as a dip in n and a peak in k, strongly increases with decreasing N. We found the lower members ($N = 1$ and $N = 2$) exhibit some of the strongest dispersions from exciton resonances among known materials. Figure 2(d) presents ε' and ε'' for $N = 1$ and $N = 2$ (results for other members are shown in Supplemental Material, Fig. S7 [22]), and Fig. 2(e) shows the absorption coefficient (denoted as α) for $N = 1$ to $N = 4$; these were calculated as $\varepsilon' = n^2 - k^2$, $\varepsilon'' = 2nk$, and $\alpha = 2\pi\varepsilon''/(n\lambda)$, respectively. Notably, both $N = 1$ and $N = 2$ exhibit negative ε' at the spectral regime where $k > n$. The negative ε' relates to strong in-plane excitonic polarization that is opposite in direction (i.e., out-of-phase) to the driving field. For $N = 3$ and $N = 4$, ε' remains positive and approaches that of $MAPbI_3$ crystals [36]. The α for $N = 1$ shown in Fig. 2(e) reveals an absorption onset wavelength of 425 nm due to band-to-band transitions, which, combined with the wavelength of excitonic absorption (518 nm), yields an exciton binding energy of 0.52 eV, consistent with an earlier report [37]. The peak α values due to exciton transitions for $N = 1$ to $N = 4$ are 3.9×10^5 cm^{-1} (at 518 nm), 3.0×10^5 cm^{-1} (at 579 nm), 2.55×10^5 cm^{-1} (at 613 nm), and 2.03×10^5 cm^{-1} (at 652 nm), respectively. As shown in Fig. 2(f), these α values translate to 5.3%, 5.7%, 6.4%, or 6.4% absorption of light with one, two, three, or four layers of perovskites in $N = 1$ to $N = 4$, respectively (together with the associated organic spacers); hence, excitonic light absorption *per perovskite layer* is strongly N dependent. Note that monolayer light absorption in $N = 1$ is weaker than that of monolayer 2D transition metal dichalcogenides (TMDs) (peak α of about 10%) [38]. However, we emphasize that in contrast to 2D TMDs, which are direct band gap only in the monolayer limit [39], high α and negative ε' in 2DHPs are bulk properties. In particular, the negative ε' realized in 2DHPs with an albeit weaker exciton resonant absorption arises from the smaller dielectric background in the visible range as compared to 2D TMDs; negative ε' cannot be achieved in the latter even in the monolayer limit [20]. The order-of-magnitude different penetration depths on and away from the exciton resonance also suggest that the commonly used diffuse reflectance technique may not yield accurate spectral shape of α vs wavelength for 2DHPs (even in arbitrary units).

To probe the out-of-plane permittivity (ε_{zz}), we performed reflectivity measurements examining the ac plane with $\boldsymbol{k}\|\vec{b}$ and $\boldsymbol{E}\|\vec{c}$ [Fig. 3(a) inset], both before and after the

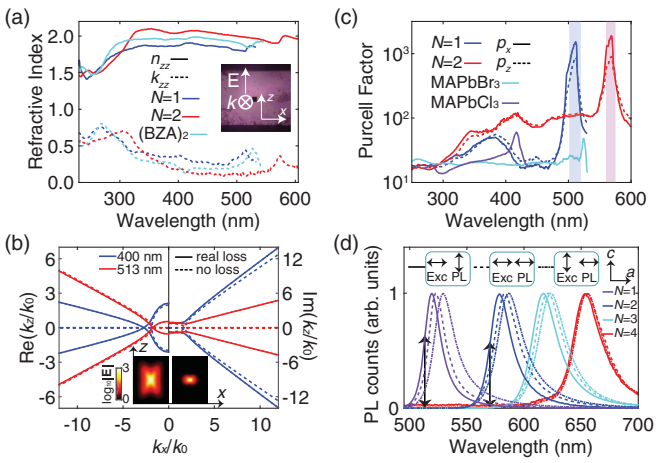

FIG. 3. (a) n and k along $\vec{c}$ for $N = 1$, $N = 2$, and $(BZA)_2PbI_4$. (b) Isofrequency curves for $N = 1$ at 513 nm (red) and 400 nm (blue) with real loss (ε'' taken to be the measured values; solid lines) and no loss (ε'' taken to be 0; dashed lines). Inset: simulated electric field amplitude produced by a dipole polarized along $\vec{x}$ (left: 513 nm; right: 400 nm) with real loss. Width and height of the plotted domain are 50 nm and 75 nm, respectively. (c) Simulated Purcell factors for 2DHPs ($N = 1$, $N = 2$), and 3D perovskites ($MAPbBr_3$ and $MAPbCl_3$). p_x and p_z denote that the dipole polarizations are along x and z directions, respectively. The colored areas highlight the hyperbolic regime (blue for $N = 1$ and red for $N = 2$). (d) Polarization-resolved PL spectra for $N = 1$ to $N = 4$ with excitation light normally incident onto the ac plane. Polarizations of the excitation light and collected PL were parallel to either $\vec{a}$ or $\vec{c}$ (inset). Double-sided black arrows indicate the center of the hyperbolic regimes for $N = 1$ and $N = 2$.

coating of MoO_x. We found the reflectivity with $\boldsymbol{k}\|\vec{b}$ and $\boldsymbol{E}\|\vec{a}$ to be the same as that measured with $\boldsymbol{k}\|\vec{c}$ under unpolarized light, as expected for a uniaxial medium. Notably, the reflectivities with $\boldsymbol{E}\|\vec{c}$, as shown in Supplemental Material, Fig. S8a [22], do not exhibit strong excitonic features as compared to those measured with $\boldsymbol{k}\|\vec{c}$. Accordingly, the determined n, k [Fig. 3(a)], and permittivities (Supplemental Material, Figs. S8b and S8c [22]] show substantially weaker dispersions near the exciton resonances. The strong excitonic anisotropy arises from the singlet nature of the in-plane excitons as compared to the out-of-plane excitons which are primarily triplet in nature, which yields a substantially different transition dipole matrix element [40].

Near the exciton transition, we observe $\varepsilon_{xx} = \varepsilon_{yy} < 0$ and $\varepsilon_{zz} > 0$ for $N = 1$ and $N = 2$ [Fig. 2(d)]. Such behavior, by definition, results in a natural type-II hyperbolic dispersion for transverse-magnetic (TM) waves [41,42]. Figure 3(b) displays the TM isofrequency curves for $N = 1$ calculated from the dispersion relation $k_x^2/\varepsilon_{zz} + k_z^2/\varepsilon_{xx} = \omega^2/c^2$ (here k_y is taken to be 0). The curve has an ellipsoidal shape at 400 nm where $N = 1$ is normally uniaxial, and turns into a hyperboloid at 513 nm (the negative peak of ε'_{xx}). Note that in both cases the shapes of the iso-frequency curves are perturbed by optical losses. Because the photonic density of states is proportional to the area of the isofrequency surface (at a given wavelength), the hyperboloidal shape near the exciton resonance signifies an enhanced photonic density of states as compared to that in the normally uniaxial regime. Type-II hyperbolic metamaterials composed of metal-dielectric multilayers based on free carrier behaviors were known to enhance the radiative decay rate of nearby quantum emitters; the latter is proportional to the local photonic density of states [43]. Here, the highly anisotropic excitonic transitions in 2DHPs produce unique photonic environments that can inherently facilitate the radiative decay of photoexcited excitons in the media. An advantage associated with the hyperbolicity in 2DHPs in comparison to that in metal-dielectric multilayers, is that the emitters are naturally embedded inside 2DHPs, guaranteeing an efficient coupling of the source to the hyperbolic modes, whereas in the latter case a finite distance between the emitter and the hyperbolic medium compromises the coupling strength especially between the emitter and high-k modes. The simulated near field at 513 nm [Fig. 3(b) inset, left], produced by an embedded point dipole emitter, exhibits a resonance-cone-like profile [41], with enhanced field strength compared to the 400-nm case [Fig. 3(b) inset, right] resulting from the enhanced density of states.

To further evaluate the density of states, we calculated the Purcell factors for 2D and 3D perovskites with finite-element simulations. As shown in Fig. 3(c), $N = 1$ and $N = 2$ exhibit Purcell factors an order-of-magnitude higher in the hyperbolic regime, compared to $MAPbBr_3$ and $MAPbCl_3$ at their band-edge emission wavelengths. Since the spatial extent of the emitting dipoles (i.e., the size of the excitons) and the nonlocal effects imposed by the finite size of unit cells (i.e., there is an upper limit on the accessible high wave vectors that is of the order of $1/a$ where a is the size of the unit cell) were not considered in the calculations, we expect that Purcell-factor values shown in Fig. 3(c) are overestimated. Regardless, relative comparisons between 2D and 3D perovskites indicate that 2DHPs are, among other reasons (e.g., tightly bound excitons in 2DHPs vs free carriers in 3D perovskites), intrinsically more suitable than their 3D counterparts for light-emitting applications, due to their faster radiative decay facilitated by the large optical anisotropy. Relatedly, 2DHPs have been shown to exhibit significantly shorter carrier lifetimes as compared to 3D perovskites [44].

We further note that the hyperbolic regimes for $N = 1$ and $N = 2$ [Fig. 2(d)] are centered at 513 and 571 nm, respectively, which are on the blue edge of the photoluminescence (PL) spectra measured with $\boldsymbol{E}\|\vec{c}$, where both the excitation light and PL photons are polarized in-plane [Fig. 3(d)]. This arises because the out-of-phase condition of the excitonic response relative to the driving electric field takes place on the blue side of the Lorentzian-type resonance [45]. However, the PL spectra measured with $\boldsymbol{k}\|\vec{b}$ [Fig. 3(d)] show different center wavelengths that depend on the polarization of either the excitation ($\boldsymbol{E}$) or emission ($\boldsymbol{E}_{\mathrm{PL}}$), and blueshifts along the line of ($\boldsymbol{E}\|\vec{c}$, $\boldsymbol{E}_{\mathrm{PL}}\|\vec{a}$), to ($\boldsymbol{E}\|\vec{a}$, $\boldsymbol{E}_{\mathrm{PL}}\|\vec{a}$), and to ($\boldsymbol{E}\|\vec{a}$, ($\boldsymbol{E}_{\mathrm{PL}}\|\vec{c}$)). This effect, which is more significant for lower members, arises from the large anisotropy in k [Figs. 2(c) and 3(a)] and the Stokes shift between the absorption and emission spectra. In going from ($\boldsymbol{E}\|\vec{c}$) to ($\boldsymbol{E}\|\vec{a}$), the penetration depth of the excitation light decreases, leading to a reduced reabsorption of the emitted light. Similarly, from ($\boldsymbol{E}_{\mathrm{PL}}\|\vec{a}$) to ($\boldsymbol{E}_{\mathrm{PL}}\|\vec{c}$), the self-absorption of PL photons also decreases. Indeed, the high α dictates that emitted photons in the hyperbolic region are strongly recycled (self-absorbed) [46], and can impact the apparent PL lifetime for this reason. However, the hyperbolic regime should present a better spectral matching with PL photons inside the material (before any reabsorption events occur). Furthermore, as demonstrated in Fig. 3(c), even though the in-plane ε' does not cross zero to support a hyperbolic dispersion in the spectral region adjacent to the hyperbolic regime, the large ε' anisotropy of 2DHPs still yields notably higher Purcell factors than those in 3D perovskites. The enhancement of radiative decay rate within and near the hyperbolic regime can, thus, suppress other nonradiative decay channels such as carrier trapping.

At room temperature, homogeneous broadening mainly due to Fröhlich scattering of carriers by polar longitudinal optical phonons determines the linewidth and magnitude of exciton resonances in 2DHPs [47,48], and hence the achievable spectral range and amplitude of negative in-plane

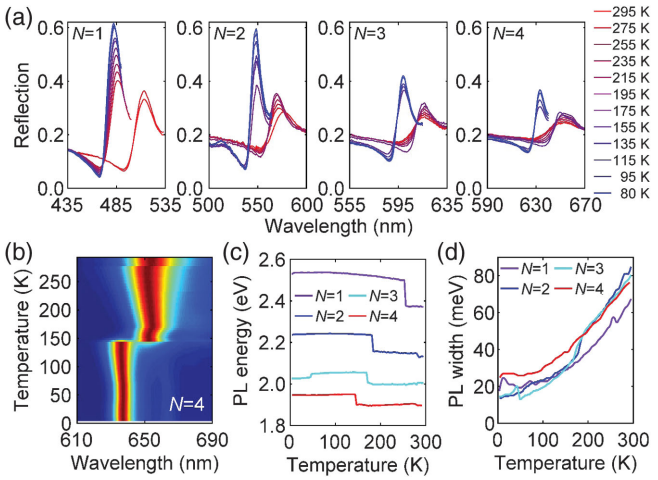

FIG. 4. (a) Temperature dependent reflectivity measured with $\boldsymbol{k}\|\vec{c}$ for $N = 1$ to $N = 4$. (b) Temperature dependent PL spectra for $N = 4$. (c) PL center energy and (d) PL full-width-half-maximum as a function of temperature for $N = 1$ to $N = 4$.

ε'. To explore excitonic linewidths and enhanced negative ε', we performed measurements at lower temperatures. As shown in Fig. 4(a), the peak reflectivities for $N = 1$ and $N = 2$ reach nearly 0.6 at 80 K, comparable in magnitude to the recently reported atomically thin mirrors based on molybdenum diselenide [49]. For $N = 3$ and $N = 4$, peak reflectivities above 0.37 can be obtained at 80 K, which are higher than the room-temperature value of $N = 1$, and suggest that negative in-plane ε' may be achievable with high members of 2DHPs at low temperatures. A nearly fourfold reduction in the full-width-half-maximum of the PL spectra for all the members [Figs. 4(b), 4(d), and Fig. S9 in Supplemental Material [22]] implies similarly narrowed linewidths of the exciton resonances, with significantly larger amplitudes of the negative in-plane ε' and smaller in-plane $|\varepsilon''|$, under the reasonable assumption that the exciton oscillator strength does not vary strongly with temperature [50]. Structural phase transitions, manifested as abrupt blueshifts of both the resonances in the reflectivity curves and the PL spectra [Fig. 4(c)], were observed for all the members.

Our work sheds light on how crystal orientations may influence the optical absorption and emission of thin-film photovoltaic and light-emitting devices with 2DHPs as the active layer. We expect that exciton-induced in-plane negative ε' can exist in various material systems including colloidal nanoplatelets [51], highly ordered organic semiconductors [52], and two-dimensional TMDs (e.g., rhenium disulfide [53]) and monochalcogenides [54] wherein excitons may be preserved in the bulk. For artificial metamaterials, the metallic and dielectric components are individually adjustable to achieve spectral and amplitude tunabilities of the negative ε'. Such tunability can be obtained in 2DHPs with (partial) substitution of the metallic cation (e.g., from Pb to Sn), the halide anion (e.g., from I to Br or Cl), or the organic spacers [55], at the atomic length scale. RI for 2DHPs with different organic spacers is discussed in the Supplemental Material [22], with the results shown in Figs. S10 to S12. Exciton-induced extreme optical anisotropy can be further conceived for polarization conversion [56], epsilon-near-zero physics [57], and strong coupling of excitons with optical cavities through the support of surface modes [58].

We thank Dr. Pierre Darancet and Dr. Stephen K. Gray for discussions, and Liliana Stan for sputtering efforts. This work was performed at the Center for Nanoscale Materials, a U.S. Department of Energy Office of Science User Facility, and supported by the U.S. Department of Energy, Office of Science, under Contract No. DE-AC02-06CH11357. Work at Northwestern University was supported by Grant No. SC0012541 from the U.S. Department of Energy, Office of Science (material synthesis). We thank the Northwestern University MRSEC (NSF DMR-1720139), and Flexterra Corp. for support of this research (MoO_x evaporation and characterization). This work made use of the J. B. Cohen X-Ray Diffraction Facility supported by the MRSEC program of the National Science Foundation (DMR-1720139) at the Materials Research Center of Northwestern University and the Soft and Hybrid Nanotechnology Experimental (SHyNE) Resource (NSF ECCS-1542205). T. X. acknowledges the support from National Science Foundation (DMR-1806152 and CBET-1150617). This material is based upon work supported by Laboratory Directed Research and Development (LDRD) funding from Argonne National Laboratory, provided by the Director, Office of Science, of the U.S. Department of Energy under Contract No. DE-AC02-06CH11357.

*schaller@anl.gov
schaller@northwestern.edu

[1] G. D. Scholes and G. Rumbles, Nat. Mater. **5**, 683 (2006).
[2] D. N. Basov, M. M. Fogler, and F. J. García de Abajo, Science **354**, aag1992 (2016).
[3] S. A. Maier, *Plasmonics: Fundamentals and Applications* (Springer, Berlin, 2007).
[4] J. D. Caldwell *et al.*, Nat. Commun. **5**, 5221 (2014).
[5] T. Low, A. Chaves, J. D. Caldwell, A. Kumar, N. X. Fang, P. Avouris, T. F. Heinz, F. Guinea, L. Martin-Moreno, and F. Koppens, Nat. Mater. **16**, 182 (2017).
[6] N. Yu, P. Genevet, M. A. Kats, F. Aieta, J.-P. Tetienne, F. Capasso, and Z. Gaburro, Science **334**, 333 (2011).
[7] J. D. Caldwell, I. Vurgaftman, J. G. Tischler, O. J. Glembocki, J. C. Owrutsky, and T. L. Reinecke, Nat. Nanotechnol. **11**, 9 (2016).
[8] H. A. Atwater and A. Polman, Nat. Mater. **9**, 205 (2010).
[9] K. V. Sreekanth, Y. Alapan, M. ElKabbash, E. Ilker, M. Hinczewski, U. A. Gurkan, A. De Luca, and G. Strangi, Nat. Mater. **15**, 621 (2016).
[10] J. Sun, N. M. Litchinitser, and J. Zhou, ACS Photonics **1**, 293 (2014).

[11] C. R. Kagan, D. B. Mitzi, and C. D. Dimitrakopoulos, Science **286**, 945 (1999).
[12] T. Ishihara, J. Takahashi, and T. Goto, Phys. Rev. B **42**, 11099 (1990).
[13] X. Hong, T. Ishihara, and A. V. Nurmikko, Phys. Rev. B **45**, 6961 (1992).
[14] K. Tanaka, T. Takahashi, T. Kondo, T. Umebayashi, K. Asai, and K. Ema, Phys. Rev. B **71**, 045312 (2005).
[15] K. Ema, K. Umeda, M. Toda, C. Yajima, Y. Arai, H. Kunugita, D. Wolverson, and J. J. Davies, Phys. Rev. B **73**, 241310 (2006).
[16] H. Takagi, H. Kunugita, and K. Ema, Phys. Rev. B **87**, 125421 (2013).
[17] G. V. Naik, B. Saha, J. Liu, S. M. Saber, E. A. Stach, J. M. K. Irudayaraj, T. D. Sands, V. M. Shalaev, and A. Boltasseva, Proc. Natl. Acad. Sci. U.S.A. **111**, 7546 (2014).
[18] C. C. Stoumpos, D. H. Cao, D. J. Clark, J. Young, J. M. Rondinelli, J. I. Jang, J. T. Hupp, and M. G. Kanatzidis, Chem. Mater. **28**, 2852 (2016).
[19] E. P. Booker *et al.*, J. Am. Chem. Soc. **139**, 18632 (2017).
[20] Y. Li, A. Chernikov, X. Zhang, A. Rigosi, H. M. Hill, A. M. van der Zande, D. A. Chenet, E.-M. Shih, J. Hone, and T. F. Heinz, Phys. Rev. B **90**, 205422 (2014).
[21] M. A. Kats, R. Blanchard, P. Genevet, and F. Capasso, Nat. Mater. **12**, 20 (2013).
[22] See Supplemental Material at http://link.aps.org/supplemental/10.1103/PhysRevLett.121.127401 for experimental methods and additional data, which includes Refs. [23–33].
[23] L. Mao *et al.*, Chem. Mater. **28**, 7781 (2016).
[24] L. Mao, W. Ke, L. Pedesseau, Y. Wu, C. Katan, J. Even, M. R. Wasielewski, C. C. Stoumpos, and M. G. Kanatzidis, J. Am. Chem. Soc. **140**, 3775 (2018).
[25] M. I. Saidaminov *et al.*, Nat. Commun. **6**, 7586 (2015).
[26] G. Maculan, A. D. Sheikh, A. L. Abdelhady, M. I. Saidaminov, M. A. Haque, B. Murali, E. Alarousu, O. F. Mohammed, T. Wu, and O. M. Bakr, J. Phys. Chem. Lett. **6**, 3781 (2015).
[27] H. Zhang, X. Liu, J. Dong, H. Yu, C. Zhou, B. Zhang, Y. Xu, and W. Jie, Cryst. Growth Des. **17**, 6426 (2017).
[28] C.-T. Lin, C.-H. Yeh, M.-H. Chen, S.-H. Hsu, C.-I. Wu, and T.-W. Pi, J. Appl. Phys. **107**, 053703 (2010).
[29] G. S. Nadkarni and J. G. Simmons, J. Appl. Phys. **41**, 545 (1970).
[30] D. J. Roth *et al.*, ACS Photonics **4**, 2513 (2017).
[31] G. Evmenenko, T. T. Fister, D. B. Buchholz, Q. Li, K.-S. Chen, J. Wu, V. P. Dravid, M. C. Hersam, P. Fenter, and M. J. Bedzyk, ACS Appl. Mater. Interfaces **8**, 19979 (2016).
[32] D. B. Buchholz, L. Zeng, M. J. Bedzyk, and R. P. H. Chang, Prog. Nat. Sci.: Mater. Int. **23**, 475 (2013).
[33] M. D. Smith, L. Pedesseau, M. Kepenekian, I. C. Smith, C. Katan, J. Even, and H. I. Karunadasa, Chem. Sci. **8**, 1960 (2017).
[34] E. S. O'Brien *et al.*, Nat. Chem. **9**, 1170 (2017).
[35] D. Hu *et al.*, Nat. Commun. **8**, 1471 (2017).
[36] A. M. A. Leguy *et al.*, Nanoscale **8**, 6317 (2016).
[37] O. Yaffe, A. Chernikov, Z. M. Norman, Y. Zhong, A. Velauthapillai, A. van der Zande, J. S. Owen, and T. F. Heinz, Phys. Rev. B **92**, 045414 (2015).
[38] D. Jariwala, A. R. Davoyan, J. Wong, and H. A. Atwater, ACS Photonics **4**, 2962 (2017).
[39] K. F. Mak, C. Lee, J. Hone, J. Shan, and T. F. Heinz, Phys. Rev. Lett. **105**, 136805 (2010).
[40] K. Tanaka, T. Takahashi, T. Kondo, K. Umeda, K. Ema, T. Umebayashi, K. Asai, K. Uchida, and N. Miura, Jpn. J. Appl. Phys. **44**, 5923 (2005).
[41] A. Poddubny, I. Iorsh, P. Belov, and Y. Kivshar, Nat. Photonics **7**, 948 (2013).
[42] P. Shekhar, J. Atkinson, and Z. Jacob, Nano Convergence **1**, 14 (2014).
[43] H. N. S. Krishnamoorthy, Z. Jacob, E. Narimanov, I. Kretzschmar, and V. M. Menon, Science **336**, 205 (2012).
[44] R. L. Milot, R. J. Sutton, G. E. Eperon, A. A. Haghighirad, J. M. Hardigree, L. Miranda, H. J. Snaith, M. B. Johnston, and L. M. Herz, Nano Lett. **16**, 7001 (2016).
[45] P. Yu and M. Cardona, *Fundamentals of Semiconductors: Physics and Materials Properties* (Springer, New York, 2010), 4th ed..
[46] L. M. Pazos-Outón *et al.*, Science **351**, 1430 (2016).
[47] A. D. Wright, C. Verdi, R. L. Milot, G. E. Eperon, M. A. Pérez-Osorio, H. J. Snaith, F. Giustino, M. B. Johnston, and L. M. Herz, Nat. Commun. **7**, 11755 (2016).
[48] Z. Guo, X. Wu, T. Zhu, X. Zhu, and L. Huang, ACS Nano **10**, 9992 (2016).
[49] G. Scuri *et al.*, Phys. Rev. Lett. **120**, 037402 (2018).
[50] B. Zhang, S. S. Kano, Y. Shiraki, and R. Ito, Phys. Rev. B **50**, 7499 (1994).
[51] S. Ithurria, M. D. Tessier, B. Mahler, R. P. S. M. Lobo, B. Dubertret, and A. L. Efros, Nat. Mater. **10**, 936 (2011).
[52] H. Najafov, B. Lee, Q. Zhou, L. C. Feldman, and V. Podzorov, Nat. Mater. **9**, 938 (2010).
[53] S. Tongay *et al.*, Nat. Commun. **5**, 3252 (2014).
[54] L. C. Gomes and A. Carvalho, Phys. Rev. B **92**, 085406 (2015).
[55] M. I. Saidaminov, O. F. Mohammed, and O. M. Bakr, ACS Energy Lett. **2**, 889 (2017).
[56] P. Ginzburg *et al.*, Opt. Express **21**, 14907 (2013).
[57] A. Alù, M. G. Silveirinha, A. Salandrino, and N. Engheta, Phys. Rev. B **75**, 155410 (2007).
[58] S. Dai *et al.*, Nat. Nanotechnol. **10**, 682 (2015).